Anadolu Üniversitesi Bilim ve Teknoloji Dergisi A- Uygulamalı Bilimler ve Mühendislik
Anadolu University Journal of Science and Technology A- Applied Sciences and Engineering

Year: 2018
Volume: 19
Number: 2
Page: 514 - 522
DOI: 10.18038/aubtda.338384

MAGNETIC MESOPOROUS SILICA NANOCOMPOSITES PREPARED WITH DIFFERENT SIZED Fe_3O_4: STRUCTURAL AND MAGNETIC PROPERTIES, CATALYTIC EFFECTS

Sezer ERDEM [1,*], Beyhan ERDEM [2], Ramis Mustafa ÖKSÜZOĞLU [3]

[1] Department of Physics, Faculty of Science and Arts, Uludağ University, Bursa, Turkey
[2] Department of Chemistry, Faculty of Science and Arts, Uludağ University, Bursa, Turkey
[3] Department of Materials Science and Engineering, Faculty of Engineering, Anadolu University, Eskişehir, Turkey

ABSTRACT

The magnetically separable mesoporous silica nanocomposites were successfully prepared through a one-pot method including the co-condensation of tetraethoxysilane (TEOS) as silica precursor and 3-mercaptopropyl trimethoxysilane (MPTMS) as functionalizing agent accompanied with hydrogen peroxide for oxidation of mercapto groups and triblock copolymers as structure directing agent in the presence of ferromagnetic and superparamagnetic Fe_3O_4 nanoparticles. By incorporating the superparamagnetic (near zero coercivity) Fe_3O_4 nanoparticles to the mesoporous silica (SBA-15) and functionalizing with sulfonic acid groups instead of ferromagnetic Fe_3O_4 nanoparticles, we developed versatile nanocomposite having superior properties with respect to magnetism, catalysis and porosity. Reducing the particle size of Fe_3O_4 from the ferromagnetic regime to the superparamagnetic regime, the pore closure could be eliminated because of the more open pore as well as saving magnetic properties.

Keywords: Magnetic nanocomposites, SBA-15, Fe_3O_4, Mesoporous silica, Esterification

1. INTRODUCTION

Mesoporous silica materials have extensive adsorption capability due to their large surface areas, and they can also be readily functionalized with acidic or basic groups via their abundant surface silanol groups [1]. In the literature, it has been reported that sulfonic acid functionalized ordered mesoporous silica catalysts have been effective for condensation and esterification reactions [2], and besides incorporating of nano-sized particles such as metal or metal oxide increases the exposed surface area of the active component of the catalyst, thereby enhancing the contact between reactants and catalyst significantly and imitating the homogeneous catalysts [3]. Moreover, mesoporous silica materials can form the stable dispersions by dispersing into the solvents. However, they can be difficult to recover, as is the case with nonmagnetic nanoparticle-supported catalysts. This problem can be overcome if the catalysts are supported on magnetic nanoparticles, especially magnetic iron oxides, that is: the catalysts can be easily recovered with the help of external magnetic field for reuse [4]. Especially, Fe_3O_4 magnetic nanoparticles have been rising as a significant useful material due to their specific properties such as superparamagnetic, non-toxic and small size etc. [5]. In nanoscale regime, there is a relationship between the size and the magnetism tuning from ferromagnetic regime (unusually large positive magnetic susceptibility) to the superparamagnetic regime (zero coercivity) [6]. According to Delaheye et al., the decreasing the size of γ-Fe_2O_3 particles down to the nanometric region enables the enhanced magnetic and chemical properties for catalytic applications which are not achieved with bulk iron oxide. There is a complex interplay between finite size effects, interface effects, and inter-particle interactions, when entering the nanometric dimension. [7].

*Corresponding Author: serdem@uludag.edu.tr
Receiving Date: 15 September 2017 Publishing Date: 29 June 2018

Biodiesel consists of C12-C22 fatty acid mono-alkyl esters, and it is a worldwide diesel fuel substitute due to its sustainable, sulfur-free, biodegradable and non-toxic properties. The esterification of fatty acids with methanol to produce biodiesel has been performed in the presence of heterogeneous acid catalysts because of their environmental and economic advantageous [8].

In the present work, the sulfonic acid functionalized magnetic Fe_3O_4-SBA-15-SO_3H composites were prepared according to a synthesis procedure of one-pot method described in the literature [9, 10] by incorporating of the ferromagnetic Fe_3O_4 (Fe_3O_4-**F**) and superparamagnetic Fe_3O_4 (Fe_3O_4-**S**) prepared by chemical co-precipitation method [11]. These magnetic composites were characterized by using N_2 adsorption/desorption, XRD, EDX, FT-IR and VSM techniques, with respect to mesoporosity, crystallography, elemental, structural and magnetism. Finally, the catalytic activities of Fe_3O_4-**F**-SBA-15-SO_3H and Fe_3O_4-**S**-SBA-15-SO_3H prepared with ferromagnetic (**F**) and superparamagnetic (**S**) Fe_3O_4 were evaluated for the esterification of oleic acid with methanol. By using superparamagnetic Fe_3O_4, we developed a versatile nanocomposite having superior properties such as magnetic, catalytic and better defined porosity compared to ferromagnetic Fe_3O_4 nanoparticles.

2. EXPERIMENTAL

2. 1. Synthesis of Magnetic Nanocomposites

Magnetic mesoporous silica nanocomposites were prepared from TEOS (Aldrich) as silica source under acidic conditions together with a structure directing agent, non-ionic triblock copolymer Pluronic 123 (Aldrich). These mesoporous silicas were modified using 3-mercaptopropyl trimethoxysilane (Aldrich) as organoalkoxysilane and mercapto groups were oxidized with hydrogen peroxide in the presence of two different sized Fe_3O_4 nanoparticles. The molar composition of the reaction components was allowed as: 0.032 Pluronic 123: 0.45 HCl: 0.15 TEOS: 0.04 MPTMS: 1.94 H_2O_2. All of the experiments were conducted under N_2 atmosphere and SBA-15-SO_3H non-magnetic catalyst was also prepared for comparison test.

2.2. Characterization

The High-Angle X-ray diffraction patterns were recorded between 10^o and 80^o in a Rigaku-rint 2200 X-ray diffractometer (XRD) with CuK_α radiation (λ = 0.154 nm). Low-Angle-XRD patterns were collected using a Rigaku Ultima IV X-ray diffractometer from 0.5 to 2.5^o (2θ). N_2 adsorption/desorption analyses were measured at 77 K with Micromeritics ASAP 2020. After being degassed at 200^oC in vacuum for 5h, the samples were measured. Magnetic properties were examined at ambient condition using a vibrating sample magnetometer (VSM, X9 Microsense) with a maximum applied field of 20 kOe. FT-IR measurements were performed using PerkinElmer Spectrum 100 series infrared spectroscopy. The components of the nanoparticles were analyzed by using energy dispersed X-ray spectrometer (EDX, Quanta-Bruker AXS).

2.3. Catalytic Test

The esterification of oleic acid with methanol was carried out in a two-necked flask one of which was equipped with a reflux condenser at 333 K temperature, 500 rpm stirring speed and 0.25 g of catalyst loading. Samples (0.5 mL) were withdrawn with an hour intervals and mixed with 2.5 mL of ethyl ether/ethanol (v/v) mixture and titrated with 0.01 M sodium hydroxide to determine the amount of unreacted oleic acid.

3. RESULTS AND DISCUSSION

N_2 adsorption/desorption isotherms of SBA-15-SO_3H, ferromagnetic and superparamagnetic Fe_3O_4 loaded SBA-15-SO_3H are compared in Figure 1a. Except some differences, all of the samples exhibit type IV isotherm concerning to mesoporous materials. The hysteresis loops become broader after Fe_3O_4 loading for both nanocomposites. The desorption branches of these isotherms shift to lower pressure. A peculiar behavior is observed on the hysteresis loops, that is: the remaining without being filled with Fe_3O_4 nanoparticles behave as usual while partially blocked mesopores result in lower hysteresis loop. In our opinion, there may be a transition from H_1 to H_2 hysteresis type suggesting the presence of smaller Fe_3O_4 particles. This change is more marked with Fe_3O_4-**F**-SBA-15-SO_3H, which gives rise to wider size range. Furthermore, larger oxide particles settled down on the outlet of the silica grains could have also plugged the mesopore entrances, in comparison with Fe_3O_4-**S**-SBA-15-SO_3H. The pore-size distribution curves (Figure 1b) obtained by using the BJH model reveal that the diameter of the mesopores decreases after Fe_3O_4 introduction. Specific surface area, pore volume and pore diameter of the samples are shown in Table 1. It can be concluded from the Table 1 that the accessible porous volume and accessible specific surface area decrease more remarkably in Fe_3O_4-**F**-SBA-15-SO_3H than those in Fe_3O_4-**S**-SBA-15-SO_3H. For catalytic applications, the accessible porous volumes and surface area are essential, because the accessibility of these parameters results in the accessibility of active sites.

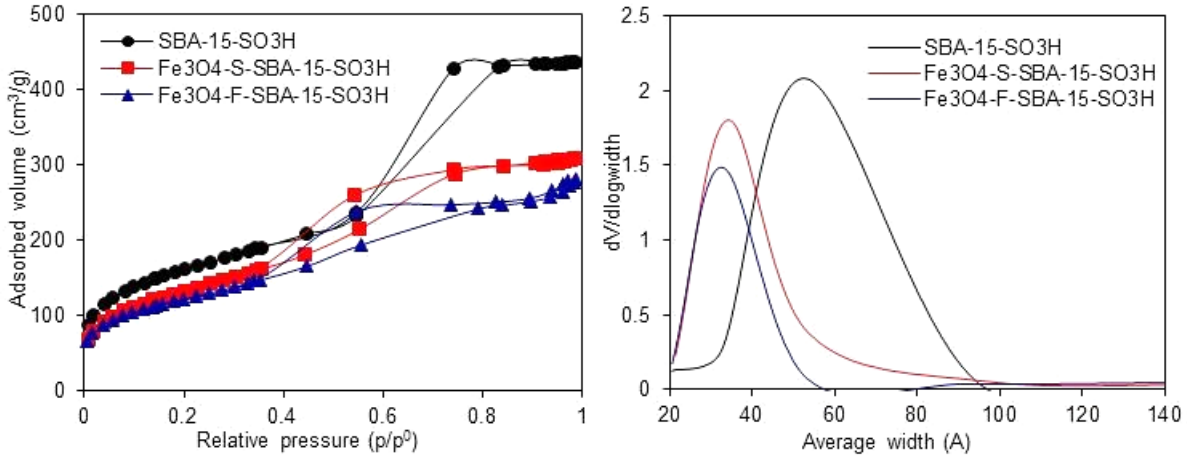

(a) **(b)**

Figure 1. N_2 adsorption/desorption isotherms of SBA-15-SO_3H, Fe_3O_4-**S**-SBA-15-SO_3H and Fe_3O_4-**F**-SBA-15-SO_3H samples (a) and their corresponding pore-size distribution curves (b).

Figure 2 shows the small-angle XRD patterns of Fe_3O_4-**F**-SBA-15-SO_3H, Fe_3O_4-**S**-SBA-15-SO_3H and bare SBA-15-SO_3H. The peak around at $2\theta \approx 0.8^o$, ascribing to (100) diffraction of hexagonal mesoporous structure with *p6mm* symmetry, is more retainable for Fe_3O_4-**S**-SBA-15-SO_3H compared with Fe_3O_4-**F**-SBA-15-SO_3H. The reduction of peak intensity demonstrates that the long range ordering decreased because of the partially clogged pores by Fe_3O_4 magnetic nanoparticles. Since the introduction of MPTMS and hydrogen peroxide during sulfonic acid functionalizing decreases the ordering of SBA-15, other diffraction peaks ((110) and (200)) disappeared in the patterns of the acid catalysts as can be seen in the literature [12]. At high angles (Figure 3a, b), all the diffraction peaks belonging to Fe_3O_4-**F** and Fe_3O_4-**S** as well as corresponding composite forms can be indexed to the inverse spinel structure of ferrimagnetic Fe_3O_4 nanoparticles [13]. Besides, the amorphous silica matrix in Fe_3O_4-**F**-SBA-15-SO_3H and Fe_3O_4-**S**-SBA-15-SO_3H samples has been revealed at $2\theta = 18\text{-}28^o$ as amorphous silica region. By applying the Scherrer formula to the XRD data, particle sizes of Fe_3O_4-**F** and Fe_3O_4-**S** and their corresponding composite forms can be estimated and given in Table 2. When this result was combined with N_2 sorption results, we concluded that the decreasing of the size of Fe_3O_4 towards the superparamagnetic region leads to the less collapsed silica architecture.

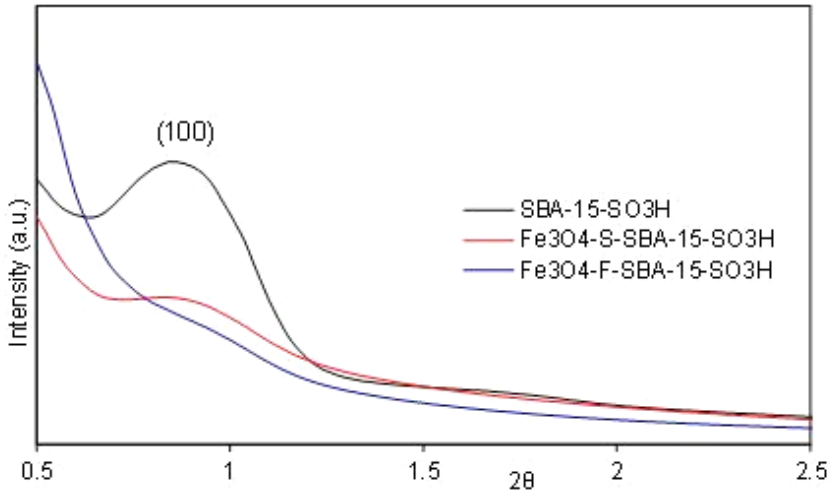

Figure 2. Low angle XRD patterns of SBA-15-SO_3H, Fe_3O_4-**S**-SBA-15-SO_3H and Fe_3O_4-**F**-SBA- 15-SO_3H.

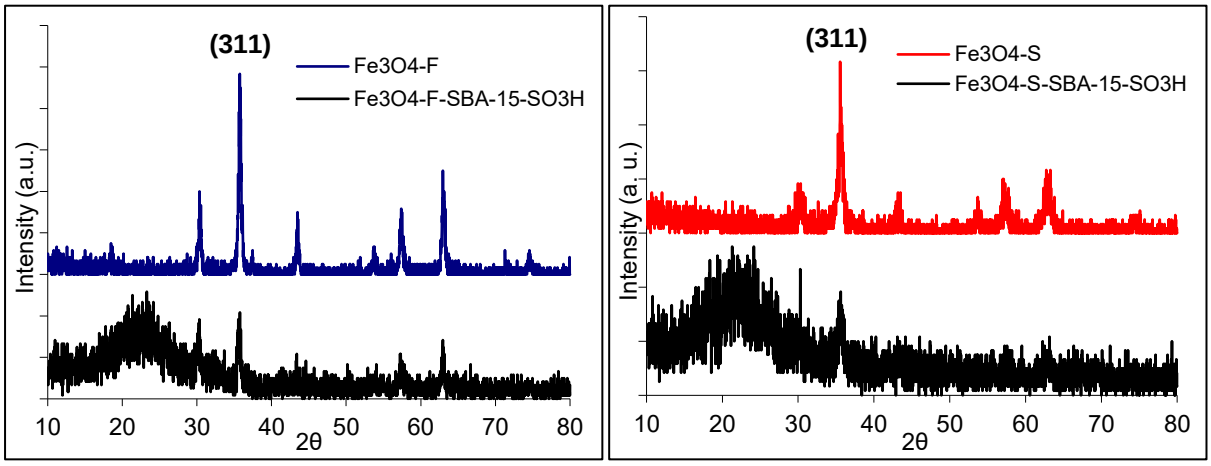

Figure 3. High angle XRD patterns of Fe_3O_4-**F** (a), Fe_3O_4-**S** (b) and their corresponding composite forms.

Table 1. Textural properties of SBA-15-SO_3H, Fe_3O_4-**S**-SBA-15-SO_3H, and Fe_3O_4-**F**-SBA-15-SO_3H.

Sample	**S_{BET} (m^2g^{-1})**	**V_{pore} (cm^3g^{-1})**	**d_{pore} (nm)**	**$\Delta S/S^0$ (accessible surface area%)[a]**	**$\Delta V/V^0$ (accessible pore volume%)[b]**
SBA-15-SO_3H	546.31	0.6344	4.797		
Fe_3O_4-**S**-SBA-15-SO_3H	463.89	0.5136	3.629	84.9	81.0
Fe_3O_4-**F**-SBA-15-SO_3H	421.56	0.4211	3.596	77.2	66.4

[a]Difference between the surface area measured before and after Fe_3O_4 loading.
[b]Difference between the pore volume measured before and after Fe_3O_4 loading.

Table 2. Magnetic and structural properties of Fe_3O_4-**S**, Fe_3O_4-**F** and their corresponding composites.

Sample	M_s (emu/g)	H_c (Oe)	Particle Size[c] (nm)
Fe_3O_4-**S**-SBA-15-SO_3H	4.1	16.03	24.6
Fe_3O_4-**F**-SBA-15-SO_3H	12.1	82.58	49.8
Fe_3O_4-**S**	61.9	5.78	25.9
Fe_3O_4-**F**	73.1	88.96	42.7

[c]By applying the Scherrer formula to (311) XRD pattern of Fe_3O_4 nanoparticles.

In order to study the magnetic behavior of Fe_3O_4-**F** and Fe_3O_4-**S** and their corresponding composite forms, magnetization measurements were performed with vibrating sample magnetometer (Figures 4 and 5). The introduction of the magnetic nanoparticles results in the reduction of the saturation magnetization (M_s) for both samples. In addition, the decrease in the magnetization for Fe_3O_4-**S**-SBA-15-SO_3H (93%) is more than that of Fe_3O_4-**F**-SBA-15-SO_3H (83%), as compared to their starting magnetic powder. This may be a consequence of the modification of superexchange interactions at Fe-O-Si surface related with particle size reduction in Fe_3O_4-**S**-SBA-15-SO_3H sample in this study. Surface effects are more obvious in the case of ferrimagnetic iron oxides with localized magnetic moments than those of the bulk oxides, due to the superexchange interaction between Fe^{3+} ions and adjacent sites in a solid via intervening O^{2-} ions [14]. In brief, the strong surface effects for Fe_3O_4-**S**-SBA-15-SO_3H composite can be directly correlated to its smaller size, compared to Fe_3O_4-**F**-SBA-15-SO_3H, which can be responsible for the modification of superexchange interactions at the surface via specific particle-silica walls interactions. As shown in the insets of Figures 4 and 5, the magnetization curves of Fe_3O_4-**S** and Fe_3O_4-**S**-SBA-15-SO_3H at room temperature do not exhibit any hysteresis, while the situation is not the same for Fe_3O_4-**F** and Fe_3O_4-**F**-SBA-15-SO_3H. As the dimension of magnetic iron oxide gets smaller (Table 2), not only the surface spins but also the internal spins begin to canting due to increased interactions between the surface and internal spins [6]. However, when we investigate the hysteresis curves in detail, a little coercivity (H_c) value was observed for Fe_3O_4-**S** (5.78 Oe) and it increased to 16.03 Oe for Fe_3O_4-**S**-SBA-15-SO_3H. It means that the effect of the surface spins is even larger for these samples because of the same reason that is: the modification of superexchange interactions. Otherwise, a reduction in the coercivity is observed for the Fe_3O_4-**F** and Fe_3O_4-**F**-SBA-15-SO_3H (from 88.96 to 82.58 Oe), but all the nanocomposites being evaluated as solid acid catalyst remained ferrimagnetic at room temperature.

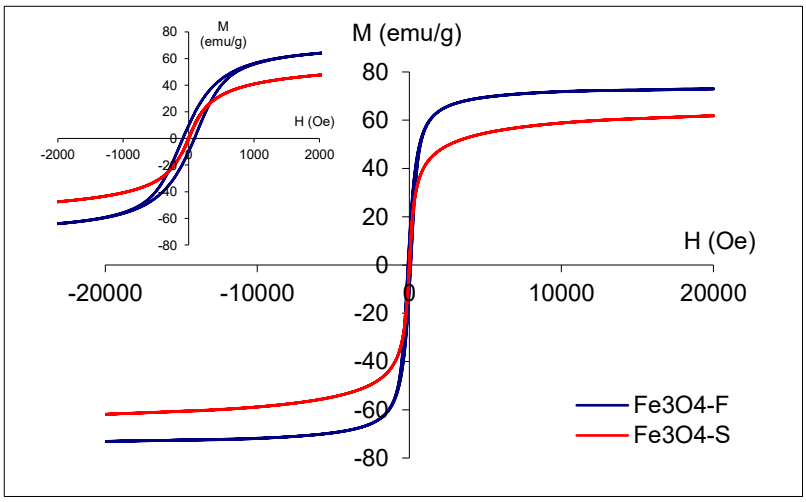

Figure 4. Magnetization curves for Fe_3O_4-**S** and Fe_3O_4-**F** at room temperature between -20 and 20 kOe (-2000 and 2000 Oe inset).

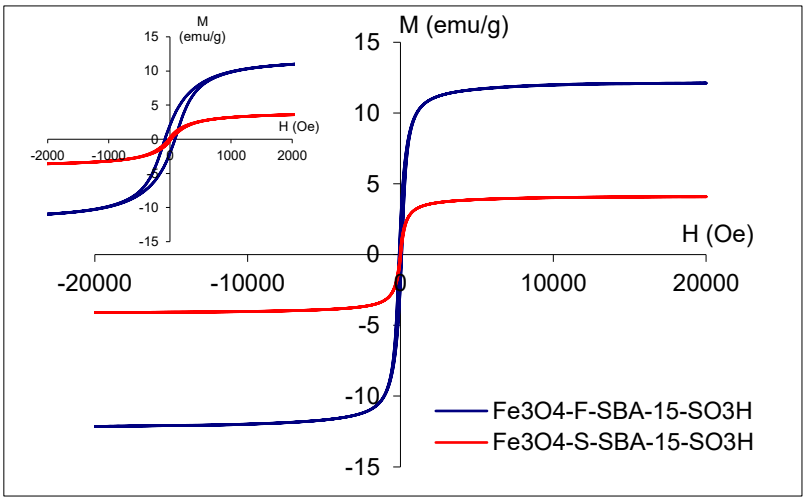

Figure 5. Magnetization curves for Fe_3O_4-**F**-SBA-15-SO_3H and Fe_3O_4-**S**-SBA-15-SO_3H at room temperature between -20 and 20 kOe (-2000 and 2000 Oe inset).

Figure 6 shows the FT-IR spectra of SBA-15-SO_3H, Fe_3O_4-**S**-SBA-15-SO_3H, and Fe_3O_4-**F**-SBA-15-SO_3H magnetic nanocomposites. The characteristic absorption peak for Fe_3O_4 is observed at 660 cm^{-1}(Fe-O bands) [15] and those of SBA-15-SO_3H are evident at 960 cm^{-1} (Si-O bending vibration), at 1080 cm^{-1} (-SO_3H groups) and 2935 cm^{-1} (C-H stretching vibration), respectively. O-H stretching vibration due to physisorbed water and potentially surface hydroxyls near 3420 cm^{-1}, and on O-H deformation vibration near 1630 cm^{-1} and Si-O stretching around at 1035 cm^{-1} are more intense for Fe_3O_4-**S**-SBA-15-SO_3H than those of Fe_3O_4-**F**-SBA-15-SO_3H, which indicates the more successfully sulfonic acid functionalization for Fe_3O_4-**S**-SBA-15-SO_3H [16]. The introduction of Fe_3O_4 to the SBA-15-SO_3H was confirmed by the bands at 585 and 630 cm^{-1} assigned to the Fe-O absorption bands. These features revealed the existence of the Fe_3O_4 species on the particles, and the spectra were in good agreement with literature [17].

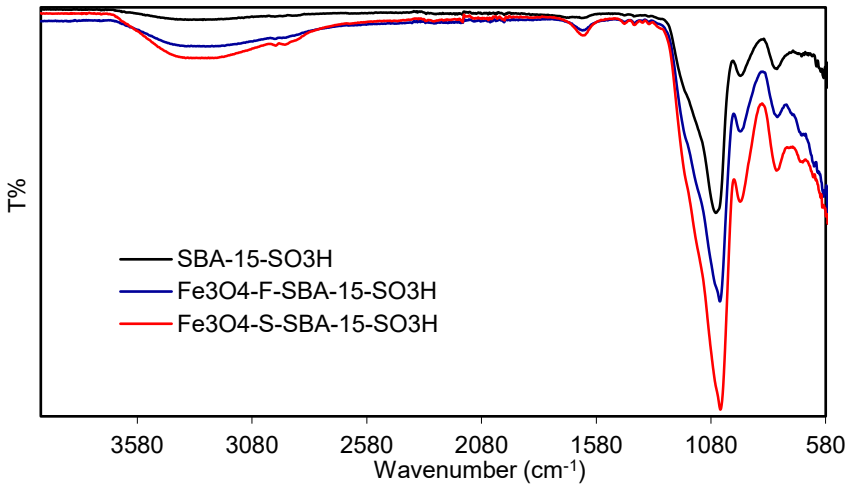

Figure 6. FT-IR spectra of SBA-15-SO_3H, Fe_3O_4-**F**-SBA-15-SO_3H and Fe_3O_4-**S**-SBA-15-SO_3H.

Figure 7 shows the elemental compositions of Fe_3O_4-**F**-SBA-15-SO_3H and Fe_3O_4-**S**-SBA-15-SO_3H composites by using energy-dispersive X-ray spectroscope (EDX). It can be concluded from the spectra that both of the magnetic nanoparticles (Fe_3O_4-**F** and Fe_3O_4-**S**) could penetrate into the mesostructure without damaging. EDX spectra reveal that Si and S peaks of Fe_3O_4-**S**-SBA-15-SO_3H composite are higher than those of Fe_3O_4-**F**-SBA-15-SO_3H composites because of better functionalization.

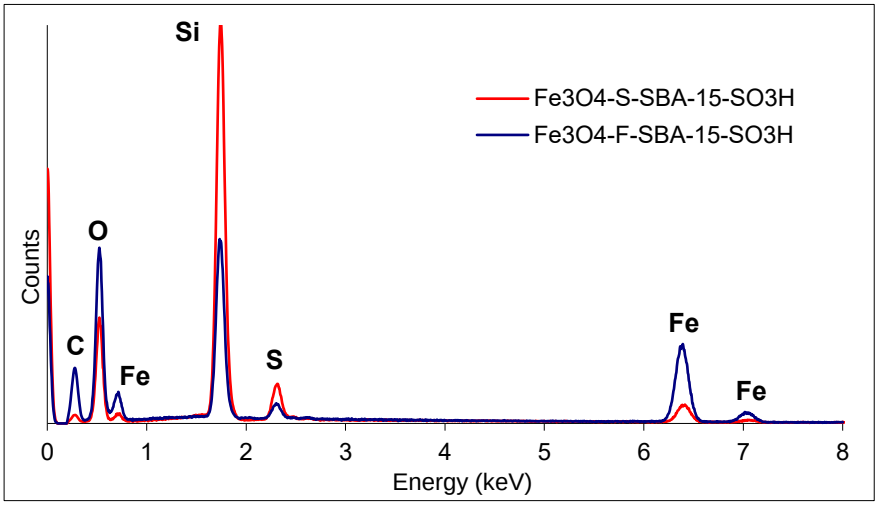

Figure 7. EDX spectra of Fe_3O_4-**S**-SBA-15-SO_3H and Fe_3O_4-**F**-SBA-15-SO_3H samples

A comparison of the catalytic behavior of the Fe_3O_4-**S**-SBA-15-SO_3H and Fe_3O_4-**F**-SBA-15-SO_3H is shown in Figure 8. Experiments were carried out under identical conditions except for the type of catalyst. The increase in the reaction rate for the larger pore-sized Fe_3O_4-**S**-SBA-15-SO_3H composite can be explained by internal pore diffusion. Since we synthesized Fe_3O_4-**F**-SBA-15-SO_3H and Fe_3O_4-**S**-SBA-15-SO_3H using identical procedures with the same loading of the mercapto groups and oxidizing agent, the different catalytic activity can be the result of the difference in pore size solely resulted in the difference in size of embedded Fe_3O_4 nanoparticles [18].

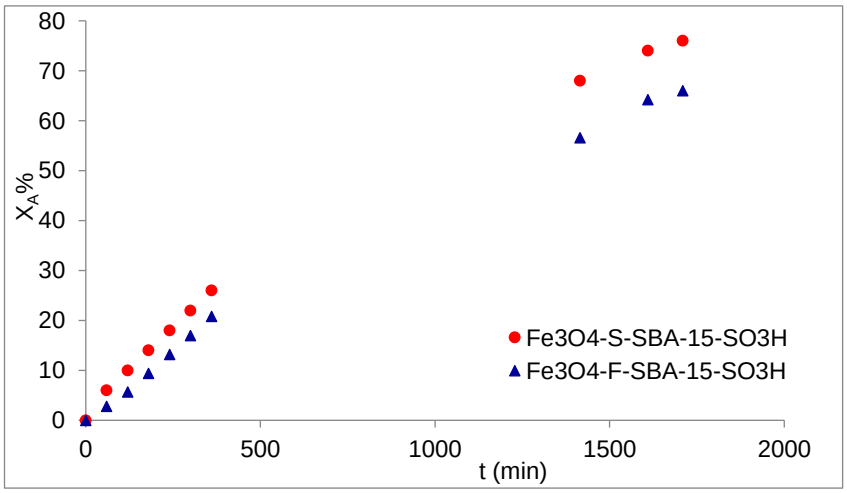

Figure 8. Esterification of oleic acid with methanol over Fe_3O_4-**S**-SBA-15-SO_3H and Fe_3O_4-**F**-SBA-15-SO_3H samples (60° C, 500 rpm, 0.25 g catalyst loading).

4. CONCLUSION

The magnetically separable mesoporous silica nanocomposites were successfully prepared through a one-pot method consisting of the co-condensation of tetraethoxysilane and mercaptopropyl trimethoxysilane and oxidation of mercapto groups in the presence of ferromagnetic and superparamagnetic Fe_3O_4 nanoparticles, triblock copolymers and hydrogen peroxide. By combining Fe_3O_4 and SBA-15-SO_3H mesoporous structure, the solid acid is not only separable from mixtures but also durable under hydrothermal conditions. Incorporating the superparamagnetic iron oxide particles which have smaller particle size to the mesoporous material resulted in larger pore size and also higher

catalytic activity. When we reduced the particle size of Fe_3O_4 to the range of superparamagnetism, we are able to eliminate the pore closure, resulted in more accessible pore as well as saving magnetic properties.

ACKNOWLEDGMENTS

This work was supported by The Commission of Scientific Research Projects of Uludag University, Project number: KUAP(F)-2014/33 and OUAP(F)-2015/21.

REFERENCES

[1] Zhu H, Shanks BH, Heindel TJ. Enhancing CO-water mass transfer by functionalized MCM41 nanoparticles. Ind Eng Chem Res 2008; 47: 7881-7887.

[2] Rhijn WMV, De Vos DE, Sels BF, Bossaert WD, Jacobs PA. Sulfonic acid functionalised ordered mesoporous materials as catalysts for condensation and esterification reactions. Chem Commun 1998; 317-318.

[3] Polshettiwar V, Varma RS. Green chemistry by nano-catalysis. Green Chem 2010; 12: 743-754.

[4] Gill CS, Price BA, Jones CW. Sulfonic acid-functionalized silica-coated magnetic nanoparticle catalysts. J Catal 2007; 251: 145-152.

[5] Dung DTK, Hai TH, Phuc LH, Long BD, Vinh LK, Truc PN. Preparation and characterization of magnetic nanoparticles with chitosan coating. J Phys Conf Ser 2009; 187: 012036 (1-5).

[6] Jun Y-W, Seo J-W, Cheon J. Nanoscaling laws of magnetic nanoparticles and their applicabilities in biomedical sciences. Acc Chem Res 2008; 41: 179-189.

[7] Delahaye E, Escax V, Hassan NE, Davidson A, Aquino R, Dupuis V, Perzynski R, Raikher YL. "Nanocasting": Using SBA-15 silicas as hard templates to obtain ultrasmall monodispersed γ-Fe_2O_3 nanoparticles. J Phys Chem B 2006; 110: 26001- 26011.

[8] Castanheiro JE, Fonseca IM, Ramos AM, Vital J. Tungstophosphoric acid immobilised in SBA-15 as an efficient heterogeneous acid catalyst for the conversion of terpenes and free fatty acids. Micro Meso Mater 2017; 249: 16-24.

[9] Lai D-m, Deng L, Li J, Liao B, Guo Q-x, Fu Y. Hydrolysis of cellulose into glucose by magnetic solid acid. ChemSusChem 2011; 4: 55-58.

[10] Erdem S, Öksüzoğlu RM, Avşar SB, Erdem B. Magnetic mesoporous silica nanocomposite for biodiesel production. Acta Phys Pol A 2017; 132: 763-766.

[11] Kassaee MZ, Masrouri H, Movahedi F. Sulfamic acid-functionalized magnetic Fe_3O_4 nanoparticles as an efficient and reusable catalyst for one-pot synthesis of α-amino nitriles in water. Appl Catal A: Gen 2011; 395: 28-33.

[12] Lai D-m, Deng L, Guo Q-x, Fu Y. Hydrolysis of biomass by magnetic solid acid. Energy & Environ Sci 2011; 4: 3552-3557.

[13] Souza KC, Salazar-Alvarez G, Ardisson JD, Macedo WAA, Sousa EMB. Mesoporous silica-magnetite nanocomposite synthesized by using a neutral surfactant. Nanotechnology 2008; 19: 185603 (1-7).

[14] Caizer C, Savii C, Popovici M. Magnetic behaviour of iron oxide nanoparticles dispersed in a silica matrix. Mater Sci Eng B 2003; B97: 129-134.

[15] Mu B, Wang T, Wu Z, Shi H, Xue D, Liu P. Fabrication of functional block copolymer grafted superparamagnetic nanoparticles for targeted and controlled drug delivery. Coll Surf A: Physicochem Eng Aspects 2011; 375: 163-168.

[16] Phan NTS, Jones CW. Highly accessible catalytic sites on recyclable organosilane-functionalized magnetic nanoparticles: An alternative to functionalized porous silica catalysts. J Mol Catal A: Chem 2006; 253: 123-131.

[17] Can K, Ozmen M, Ersoz M. Immobilization of albumin on aminosilane modified superparamagnetic magnetite nanoparticles and its characterization. Coll Surf B: Biointerfaces 2009; 71: 154-159.

[18] Jun SW, Shokouhimehr M, Lee DJ, Jang Y, Park J, Hyeon T. One-pot synthesis of magnetically recyclable mesoporous silica supported acid-base catalysts for tandem reactions. Chem Commun 2013; 49: 7821-7823.